Journal of Solid Mechanics Vol. 15, No. 1 (2023) pp. 90-108
DOI: 10.22034/jsm.2022.1947318.1721

Research Paper

Dynamic and Quasi-Static Plastic Behavior of Single and Nested Thin-Walled Square Tubes Under Lateral Loading

B. Shabani [1], S. Gohari Rad [2], A. Alijani [1,*], R. Rajabiehfard [2]

[1]*Department of Mechanical Engineering, Bandar Anzali Branch, Islamic Azad University, Bandar Anzali, Iran*
[2]*Department of Mechanical Engineering, Rasht Branch, Islamic Azad University, Rasht, Iran*

Received 5 November 2022; accepted 4 January 2023

ABSTRACT

This paper investigates the dynamic and quasi-static plastic behavior of single and nested mild steel square tubes under lateral loadings experimentally and numerically. The dynamic experimental tests are carried out using a gas gun and the dynamic force-time responses are measured with a load cell. Also, the quasi-static experimental tests are performed in a universal test machine. The dynamic experimental tests are also simulated with the finite element software Abaqus. Furthermore, the square tubes' combinations in the nested systems are investigated in the present work. It is revealed that the amount of peak load decreases significantly when the form of the single tube changes from square to lozenge. It is also observed that in the nested tube structures, by changing each of the outer or inner tubes or both of them from the square form to lozenge one, the amount of peak load decreases meanwhile the energy absorption capacity decreases too, which is not desirable for energy absorbers. By comparing the impact results of both the single and nested square tubes which have the same mass, it can result that the nested square tubes behave better as energy absorbers compared with the single tubes.

Keywords : Single and nested square tubes; High rate and quasi-Static lateral loading; Experimental and numerical investigation; Energy absorption; Gas gun.

1 INTRODUCTION

THIN-WALLED structures are widely used in different engineering fields due to their high energy absorption capacity, simplicity in structure and low cost. Thus, during the last few decades, a significant number of investigations on thin-walled structures have been conducted. These studies can be classified into several categories. Different cross-sections of thin-walled tubes (circular, square, triangle, etc.) [1-4], different tube materials (steel, aluminum, composite, etc.) [5-9], and also different loading conditions such as quasi-static [2,4,8,10] and impact loading [1,3,9,11,12] are some of the important categories mentioned above. The studies can also involve another

*Corresponding author. Tel.: +98 9111351067; Fax: +98 1333730223.
E-mail address: alijani@iaubanz.ac.ir (A.Alijani)

two important categories; loading type of tubes such as axially [1,2,6,7] or laterally [8,9,12-16] and the thin-walled tube combinations as nested ones [8-10,12,16-22]. It is also worth to mention that all the above categories can contain filled thin-walled tubes with different infill materials [15,23-26]. Gupta et al. [27] presented an experimental and computational study of rectangular and square tubes made of aluminum and mild steel which are subjected to quasi-static transverse loading. Mechanics of deformation process, comparison of experimental and computed results and the effect of process parameters on the mode of deformation discussed in this paper. Gupta et al. [28] also introduced experimental and computational analyses of circular tubes under lateral compression. Issues such as the basic deformation mechanism and the effects of process parameters on deformation behavior of the structures are discussed in this paper. Morris et al. [10] studied the quasi-static lateral compression of nested systems with vertical and inclined side constraints numerically and experimentally. The force-deflection response of mild steel short tubes compressed using two types of indenters is examined. The variation in response due to the mentioned indenters and external constraints and how these can contribute to an increase in the energy absorbing capacity of such systems are illustrated in this paper. Olabi et al. [12] investigated the behavior of the nested tube structures under lateral impact loading with and without side constraints experimentally and numerically. Remennikov et al. [23] studied the comparative behavior of square hollow section (*SHS*) tubes filled with rigid polyurethane foam (*RPF*) and concrete under low velocity lateral impact using a drop hammer. The tests were performed on mild steel and stainless steel *SHS*s for both filled and unfilled constructions. It was concluded that the concrete filled tubes had the highest impact resistance and energy absorption capacity, followed by the steel tubes filled with *RPF*, and then the hollow tubes. The results also show that *RPF*s can be used as an effective infill material in structural steel hollow columns when expedient enhancement of the energy absorption capacity is required, e.g., to increase blast and impact resistance of hollow structural elements. Alavi Nia et al. [4] investigated the effect of collapse initiators on energy absorption characteristics of square tubes under oblique quasi-static loads experimentally and numerically. Results show that collapse initiators in most of the specimens change deformation mode from general buckling to progressive buckling and decrease considerably the peak load; therefore increase crush force efficiency. Wang et al. [16] presented a theoretical, numerical and experimental investigation into the dynamic behavior of internally nested tube systems subjected to lateral impact loading in a drop hammer. It is found that by using the two-tube system and three-tube system, the force-time curves of these systems exhibit a staircase pattern, due to the contacts between the tubes. Therefore, one can obtain desirable stepwise energy absorbers by designing the geometry, material constants of each tube and the number of tubes. Baroutaji et al. [29] investigated the energy absorption behavior and crashworthiness optimization of short length circular tubes under quasi-static lateral loading. They found out that the specific energy absorption of circular tubes under lateral loading increases with increasing thickness and decreasing diameter. They also pointed out that the tubes with smaller width (W) and diameter (D) and higher thickness are more suitable as energy absorbants. Baroutaji et al. [19] in another paper presented the responses of nested tube systems under quasi-static and dynamic lateral loading. They revealed that the quasi-static and dynamic responses of the nested systems were comparable under an experimental low velocity (v=4.5 *m/s*) due to insignificant strain rate and inertia effects of the nested systems under the applied velocity. Tran and Ton [14] investigated the crushing behaviors of rectangular and square tubes under quasi-static lateral loading experimentally and theoretically. They revealed that the average crushing force of the rectangular tube is smaller than that of the square one. It was also concluded that although having different geometries, these two types of tubes have an identical crushing mechanism including two crushing stages. Pirmohammad et al. [2] investigated the crashworthiness capability of multi-cell devices subjected to axial and oblique quasi-static loads experimentally and numerically. Hu et al. [22] explored the dynamic deformation behaviors of the internally nested hemispherical shell system (*INHSS*) experimentally (in a drop hammer machine) and computationally. Results show that the dynamic deformation process and energy absorption capability of the *INHSS* depends on the thickness and radius of the inner shell. Yu et al. [21] investigated a triple-tube system (*TT*) in order to develop an efficient energy absorption component for protecting structures against blast shock. The performance of the triple-tube system studied experimentally and numerically and compared with that of a double-tube system (*DT*) and a single-tube system (*ST*). The results show that the *TT* system can provide the highest energy absorption efficiency and the most stable deformation mode, so as to enhance energy absorption capacity for protecting structures. Tran [17] studied the crushing response of the nested rectangular-square tube structures under quasi-static lateral loading experimentally and theoretically. They found out that the mean crushing load depends on the length of the plastic hinge line, wall thickness and flow stress of material. The predicted values of mean crushing load obtained from the suggested theoretical model appear to be in good agreement with the experimental data in this paper. Kahraman and Akdikmen [8] investigated the deformation behavior and energy absorption capability of nested steel tubes under quasi-static lateral loading, experimentally. Experiments were carried out on nested tube samples in which a minimum of 2 and a maximum of 6 tubes were used together in different numbers and sequences. It was determined that the sample with 5 tubes yielded the most

efficient design when specific energy absorption capability, work effectiveness, and energy efficiency parameters were considered. Shabani et al. [9] investigated the dynamic plastic behavior of single and nested circular rings using a gas gun. It was revealed that the employed single rings as energy absorbers are absorbing input energies while transmitting small amounts of forces particularly peak loads to protected specimens or occupants. Moreover, it was determined that circular rings having smaller thicknesses and greater inner diameters are much more efficient energy absorbers. However, it was found that single rings have low energy absorption capacity leading to high peak loads for high input energies. It was also concluded that nested rings can be used as suitable alternatives since they can absorb much more energy and transmit much fewer forces compared to single rings.

As it was mentioned above, most of the previous studies concentrated on deformation behavior and energy absorption capacity of the single and nested tubes subjected to the quasi-static and moderate strain rate loading conditions. Therefore, the present paper is going to investigate the behavior of the single and nested square tubes under high rate lateral loading condition by employing a gas gun in order to compensate for the few studies on the high rate lateral impact loadings. Furthermore, the finite element software Abaqus is utilized to numerically compare the dynamic plastic behavior of the single and nested thin-walled square tubes subjected to high rate lateral impact loadings with the experimental results. In the following, the geometrical properties and material specifications of the single and nested square tubes, experimental procedure, numerical simulations and finally the experimental and numerical results will be discussed.

2 SINGLE AND INTERNALLY NESTED SQUARE TUBES

The single and nested square tube specimens which are made of mild steel, are classified and illustrated in Fig. 1 according to the cross-section size of the tubes, different types of the nested tube systems and the tubes' directions in which they are subjected to the lateral loading which leads the single tube or the outer one in the nested system to be placed in the square or lozenge form in the gas gun or in the universal test machine. The tube material properties are determined according to section 4. It is also needed to mention that all the specimens (single tubes and each of the tubes in the nested system) have the same thickness and length of 2 *mm* and 30 *mm*, respectively. Table 1 and Table 2 illustrate the geometrical properties of the single and nested tubes in details, respectively.

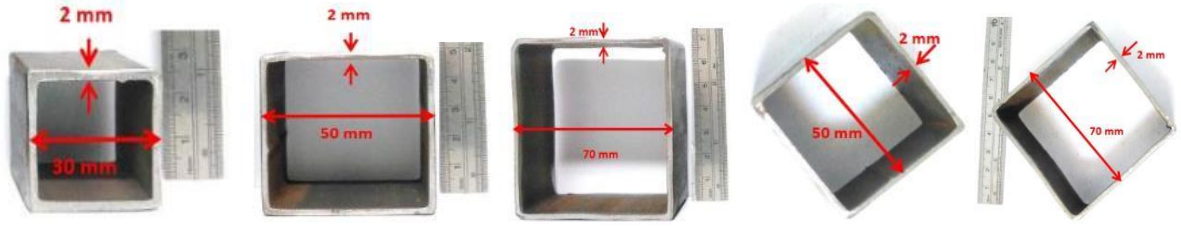

Fig.1
The geometrical properties of (a) The single square tubes and (b) The nested ones.

3 EXPERIMENTAL PROCEDURE

All the single and nested specimens and the other devices used in the experimental apparatus should be carefully prepared before the experiments. As it was mentioned in the previous sections, the single and nested square tube

specimens are subjected to the quasi-static lateral loading utilizing the universal test machine in Islamic Azad university of Lashtenesha-Zibakenar branch which is shown in Fig. 2 and they are also subjected to the dynamic lateral impact loadings in the gas gun shown in Fig. 3. In order to perform the dynamic tests in the gas gun, the specimen is located at one side and the striking mass in located at the other side. When the striking mass is shot to the specimen, a load cell which has the load capacity of 300 *kN*, is provided to measure the force at the clamped end of the tube specimen. In order to better understand the load cell performance, it should be noted that the employed load cell measures the voltage variation caused by impact using its own strain gauges. Then the measured voltage versus time is amplified with an amplifier and afterward the mentioned curve is recorded in a digital storage system named oscilloscope. Finally, the voltage-time responses can be converted to the force-time ones using a scale factor of $1mv = 79\times10^{-3}kN$. It should be noted that all the force-time curves plotted in the present paper are smoothed by using the relation $0.2\times$ the raw data $+\ 0.8\times$ the force value in the previous time step. A schematic diagram of the dynamic experimental setup is shown in Fig. 4. In the dynamic tests, all the specimens are subjected to a projectile with a mass of 0.26 *kg* which is shown in Fig. 5. The diameter and the length of the striking mass are 41 *mm* and 130 *mm*, respectively. It should be mentioned that the striking mass is made of VCN150 steel covered with Ertalon as the outer surface. Fig. 6 shows some single and nested tube specimens before and after being laterally deformed both in the gas gun and in the universal test machine. It is also needed to emphasize that all the quasi-static and dynamic tests are conducted twice to obtain the reliable results.

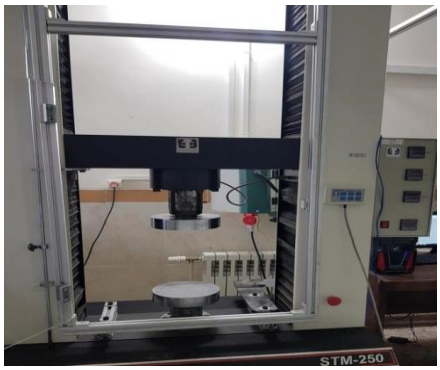

Fig.2
The universal test machine.

Fig.3
The gas gun.

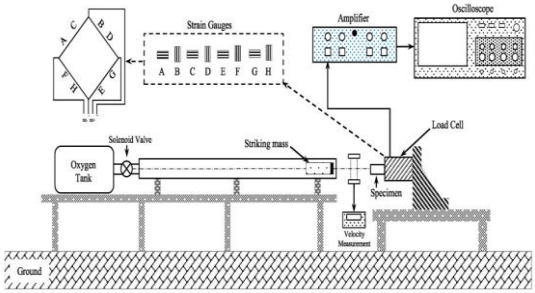

Fig.4
A schematic diagram of the dynamic experimental setup.

Fig.5
The striking mass in the dynamic experimental apparatus.

(a)

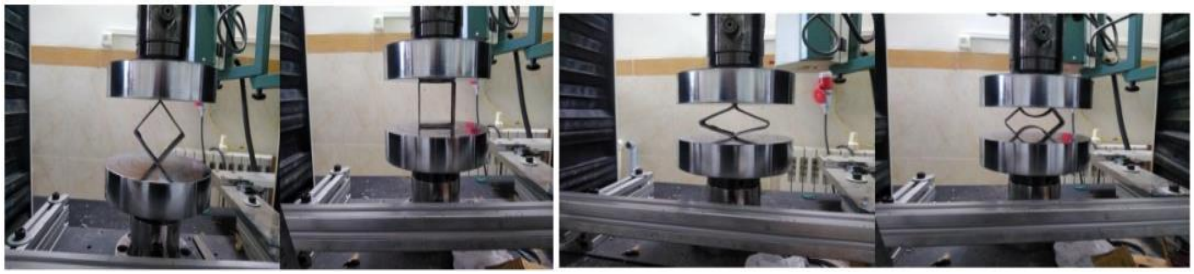

(b-1)

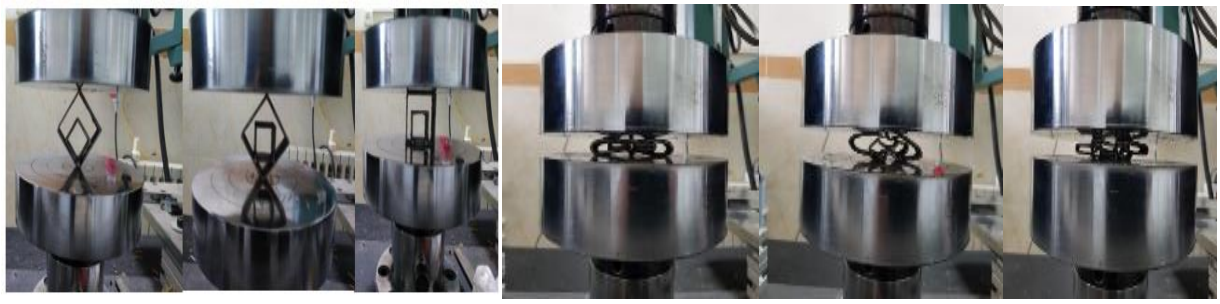

(b-2)

Fig.6
Single and nested tube specimens before and after being laterally deformed (a) in the gas gun and (b-1) and (b-2) in the universal test machine.

4 FINITE ELEMENT SIMULATIONS

The simulation of single and nested square tubes being laterally impacted is done using the finite element software Abaqus in the present work. In the simulations, as in the reality, the simulated specimen is fixed to a rigid surface at one side and it is subjected to a striking mass at the other side according to Fig. 7 which shows a view of assembled model at the moment in which the tube is impacted by the striking mass. It is obvious from Fig. 7 that the central axis of the tube specimen (single or nested one) is parallel to the rigid surface not perpendicular to it due to the simulation of lateral type loading condition. In the numerical simulations, the striking mass is shot to the tube

specimen with a given velocity while its central axis is perpendicular to the central axis direction of the single or nested tube as shown in Fig. 7. It is also needed to note that the wall which the tube specimen is fixed on and the striking mass are assumed to be rigid. Furthermore, the element type of meshing is chosen to be *C3D8R* and the mesh size is considered 0.5 *mm* in order to have converging results. Also, the contact type between all surfaces is assumed to be a general contact. In order to consider the elastic-plastic behavior of the single and nested square tubes in the *FE* simulations, the Johnson-Cook equation is employed. It is also important to mention that the Johnson-Cook equation is widely used in the simulation of high rate impact loading processes [30-34] because it includes both the effects of strain rate and strain hardening. The mentioned constitutive equation that can describe the flow stress for a variety of materials is formulated as follows [30]:

$$\sigma_d = \left[A + B\left(\varepsilon_P\right)^n\right]\left[1 + C\ln\left(\frac{\dot{\varepsilon}}{\dot{\varepsilon}^0}\right)\right] \tag{1}$$

where σ_d, A, ε_P, $\dot{\varepsilon}$ and $\dot{\varepsilon}^0$ are dynamic yield stress, initial yield stress, plastic strain, strain rate, reference strain rate, respectively and B, n and C are the model parameters which are usually defined by the experiments. It is needed to mention that the material parameters of Johnson-Cook constitutive model A, B, C and n are respectively equal to $291.96\times10^6\left(\frac{N}{m^2}\right)$, $304.98\times10^6\left(\frac{N}{m^2}\right)$, 8.62×10^{-5} and 135.09×10^{-3} which are reported for mild steel material [30]. Also, the density, elastic modulus and Poisson's ratio are equal to $7864\left(\frac{kg}{m^3}\right)$, $200\times10^9\left(\frac{N}{m^2}\right)$ and 0.30, respectively [30]. It should also be noted that although considering the experimental boundary condition of the specimens in the numerical simulations, but the most important crashworthiness parameters of energy absorbers aren't affected by the boundary condition and the loading type significantly [35-38].

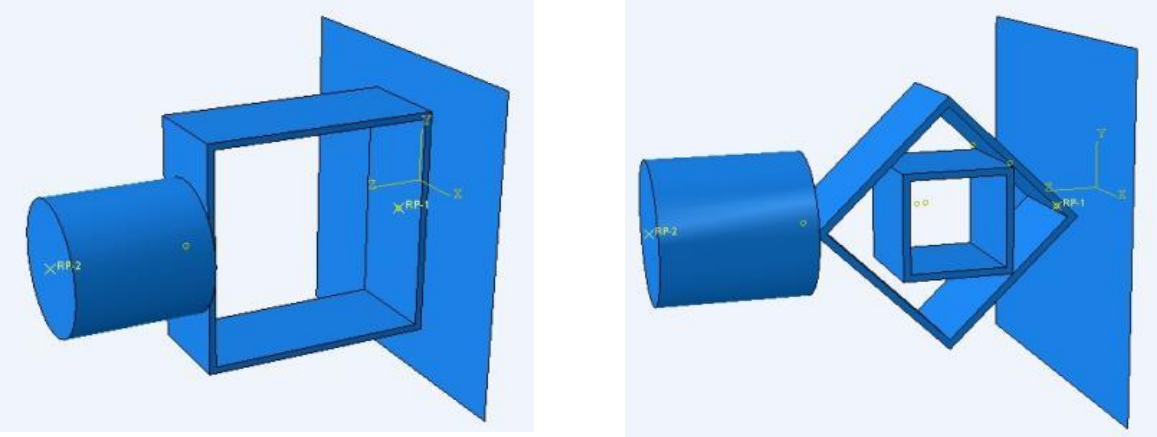

Fig.7
A view of assembled model at the moment in which the tube is impacted by the striking mass in FE simulation.

5 THEORETICALANALYSIS

To efficiently evaluate the crushing resistance of the square tubes, an analytical derivation is carried out to directly estimate the mean crushing force (MCF) of the structures. The Simplified Super Folding Element (SSFE) theory was extensively used to investigate the crushing characteristics of the energy absorber [39-40] and it was also adopted in this study. The wavelength ($2H$) of each fold is assumed constant during the progressive folding of the square tubes. By considering the energy equilibrium of the system, the external work done by the crushing force is equal to the sum of energy dissipation in bending and membrane deformation. Therefore, the external work can be defined as:

$$MCF.2H_k = E_b + E_m \tag{2}$$

where E_b and E_m are the bending energy and membrane energy, respectively; $2H$ is the wavelength of each fold, k is the effective crushing distance coefficient. According to the study of Abramowiczand and Jones [41], the length of the fold is smaller than $2H$, because the panel is not completely flattened. Moreover, the experimental results revealed that the effective crushing distance coefficient k was found between 0.7 and 0.8 [41]. Therefore, the coefficient k is set to be 0.75 in the analysis of this paper.

5.1 Bending energy

The bending energy of each fold during the crushing process can be determined by summing up the energy dissipation at three plastic stationary hinge lines. For a complete fold, the bending energy is defined as follows:

$$E_b = \sum_{i=1}^{4} M_0 \theta_i L_c \tag{3}$$

where L_c and θ_i represent the total length of all flanges and the rotation angle around the plastic i^{th} hinge, respectively. M_0 is the fully plastic bending moment per unit length, and is determined as $M_0 = \sigma_0 t^2/4$, in which σ_0 is the flow stress of the material, and t is the tube thickness. The flow stress σ_0 is computed as follows $\sigma_0 = (\sigma_y + \sigma_u)/2$ where σ_y is the yield strength, and σ_u is the ultimate strength at the strain rate [42]. It is assumed that four hinge lines completely flat after crushing, thus, the rotation angles for four hinges are $\pi/2$, π, $\pi/2$ and π respectively. Consequently, the bending energy can be expressed as follows:

$$E_b = 3\pi M_0 L_c \tag{4}$$

5.2 Membrane energy

The crushing behavior of the right corner element has been analysed by Chen and Wierzbicki [39]. The membrane energy of the right corner element during one folding wavelength is estimated as follows [39-40]:

$$E_{m,sym}^{right-corner} = \frac{4M_0H^2}{t}\left(for\ \ asymmetry\ \ deformation\right) \tag{5}$$

$$E_{m,sym}^{right-corner} = \frac{8M_0H^2}{t}\left(for\ \ asymmetry\ \ deformation\right) \tag{6}$$

5.2.1 Four-panel element

The membrane energy dissipated during one wavelength of crushing can be archived by the four-panel angle element model proposed by Zhang and Zhang [43]. The energy could be divided into two components: central-panel (at up and down) and the other 2-panel. For the central panel, the membrane energy can be defined as:

$$E_m^{central-panel} = \int_s \sigma_0 t ds = 2\sigma_0 t H^2 \tan(\alpha/2) = 8M_0 \frac{H^2}{t}\tan(\alpha/2) \tag{7}$$

By considering the influence of central angle on the crush resistance of the 2-panel angle element, the membrane energy of the element with central angle 2α can be expressed as:

$$E_m^{2-panel} = \frac{4M_0H^2\tan\alpha}{t(\tan\alpha + \frac{0.05}{\tan\alpha})/1.1} \tag{8}$$

Therefore, the total membrane energy of the 4-panel element can be calculated as:

$$E_m^{4-panel} = 2E_m^{central-panel} + E_m^{2-panel} = \frac{4M_0H^2}{t}\left(\frac{\tan\alpha}{\frac{\left(\tan\alpha+\frac{0.05}{\tan\alpha}\right)}{1.1}} + 4\tan(\alpha/2)\right) \quad (9)$$

5.3 Mean crushing force

The MCF of the square tubes depends on the number of each element in their profile. Therefore, the energy equation (Eq. (2)) can be written as:

$$MCF.2H_k = 3\pi M_0 L_c + N_1 E_m^{central-panel} + N_2 E_m^{2-panel} \quad (10)$$

where N_1 and N_2 are the number of corner elements and center elements, respectively.

6 RESULTS AND DISCUSSION

This section first investigates the deformation behavior of single square tubes under lateral quasi-static and dynamic loadings, then the deformation behavior of nested square tubes is discussed under lateral quasi-static and dynamic loading conditions and finally the crashworthiness properties of both the single and nested tubes will be compared with each other.

6.1 Single square tubes

In this part the deformation mechanism and energy absorption capacity of the single square tubes which are laterally affected by the quasi-static and dynamic loadings are studied and the experimental and numerical results will be discussed in the following.

6.1.1 Quasi-static loading condition

As it is obvious in Table 1, all the specimens *S-1*, *S-2*, *S-3*, *L*-1 and *L-2* have the same thickness and length of 2 *mm* and 30 *mm*, respectively. In order to investigate the effect of tube geometrical properties on deformation behavior, the outer side length of the square tube cross-section assigns the values of 30 *mm*, 50 *mm* and 70 *mm* to itself. Also, the outer side length of the lozenge tube cross-section gets the values of 50 *mm* and 70 *mm*. In the quasi-static experimental tests, the deformation rate is determined as 20 *mm/min*. Experimental results of the quasi-static tests conducted in the universal test machine, are presented in Table 3 which contains the experimental amounts of peak load, mean crushing force and axial displacement at peak load. It is needed to mention that the axial displacement of the tube is equal to the displacement of the upper jaw in the universal test machine. Fig. 8 presents the experimental shapes of the single square and lozenge tubes after being laterally compressed in the universal test machine. The experimental quasi-static force-displacement and force-time curves for the specimens *S-1*, *S-2*, *S-3*, *L-1* and *L-2* under lateral compression, are also depicted in Fig. 9. It is revealed that in the single square tube specimens (*S-1*, *S-2* and *S-3*) when subjected to lateral quasi-static loading, the amount of peak load decreases by increasing the side length amount of the tube hollow square cross section. It is needed to say that the amount of load reaches to its own maximum value which referred to as peak load, in the more displacement amounts when the side length amount of the square tube cross section increases. Furthermore, the mean crushing force which is equal to the crushing energy divided by the tube shortening length, is decreasing until the formation of the plastic hinge. The obtained results can also be generalized to the single tubes which are subjected to the lateral quasi-static compression in the lozenge form (specimens *L-1* and *L-2*). By considering the experimental quasi-static force-displacement responses of the samples *S-3* and *L-2* which are laterally compressed, it can be concluded from Fig. 10 that the peak load amount of the single

square tube (sample S-3) is much more than that of the single tube in the lozenge form (sample *L-2*), because the contact surface between the specimen and the upper jaw of the universal test machine in the sample *S-3* is much more than that of the lozenge form tube which is just a lateral edge. Thus, the energy needed for plastic deformation in sample *S-3* is more than that of sample *L-2*. As it is obvious, the samples *S-3* and *L-2* are totally like each other geometrically except the lateral direction of being compressed in the universal test machine. Although decreasing the peak load amount is desirable in energy absorbers, but in the case of the lozenge tube discussed above, this reduction is accompanied by the low amount of energy absorption meaning that the lozenge tube reaches its maximum energy absorption capacity under low amounts of loadings which causes the square tubes to be better as energy absorbers comparing with the lozenge ones.

S-1 *S*-2 *S*-3 *L*-1 *L*-2

Fig.8
The experimental shapes of the single square and lozenge tubes after being laterally compressed in the quasi-static loading condition.

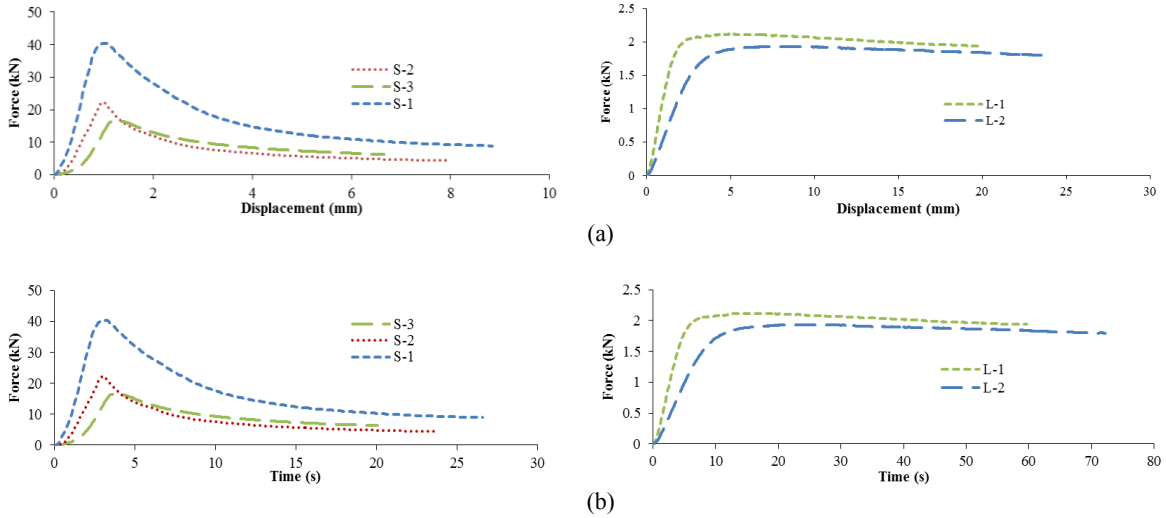

Fig.9
The experimental (a) force-displacement and (b) force-time curves for the specimens *S*-1, *S*-2, *S*-3, *L*-1 and *L*-2 subjected to quasi-static lateral loading.

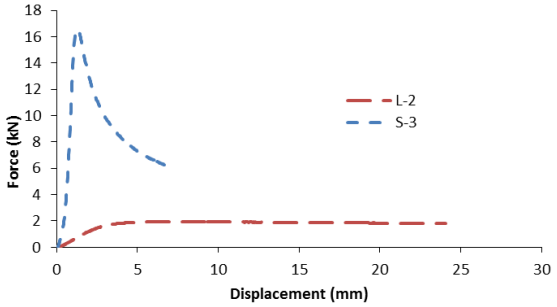

Fig.10
Experimental comparison of the force-displacement responses for the samples *S*-3 and *L*-2 under quasi-static lateral loading condition.

6.1.2 Dynamic loading condition

Among all the single tubes mentioned earlier (specimens *S-1*, *S-2*, *S-3*, *L-1* and *L-2*), this part is focused on the dynamic behavior of the specimen *S-3* which is subjected to lateral high rate impact loading experimentally and numerically. According to Table 1, the projectile mass is 0.26 *kg* and the impact velocities are 35 *m/s* and 49 *m/s*. Also, the tube specimen chosen here (*S-3*), has a mass of 0.156 *kg*. The selection of the single square tube specimen *S-3* for dynamic tests in this section is done by aiming to reasonably compare its dynamic behavior and crashworthiness characteristics with those of the nested tubes (discussed in the subsequent sections) which all have the same mass of 0.156*kg* as the specimen *S-3*. The dynamic experimental and numerical results of the specimen *S-3* including the axial displacement, peak load and the mean crushing force are presented in Table 3. The experimental and numerical deformed shapes and force-time responses and also the numerical energy absorption versus axial displacement of the specimen *S-3* subjected to high rate lateral loadings, are presented in Fig. 11.

Table 1
The geometrical properties of the single square tubes and the quasi-static and dynamic loading conditions.

Model	The properties of the single square tubes				Quasi-static test	Dynamic test	
	Material	Wall Thickness (*mm*)	Outer side length of the hollow square cross section (*mm*)	Tube length (*mm*)	Deformation rate (*mm/min*)	Projectile mass (*kg*)	Projectile velocity (*m/s*)
S-1	Mild steel	2	30	30	20	---	---
S-2		2	50	30		---	---
S-3		2	70	30		0.26	35 & 49
L-1		2	50	30		---	---
L-2		2	70	30		---	---

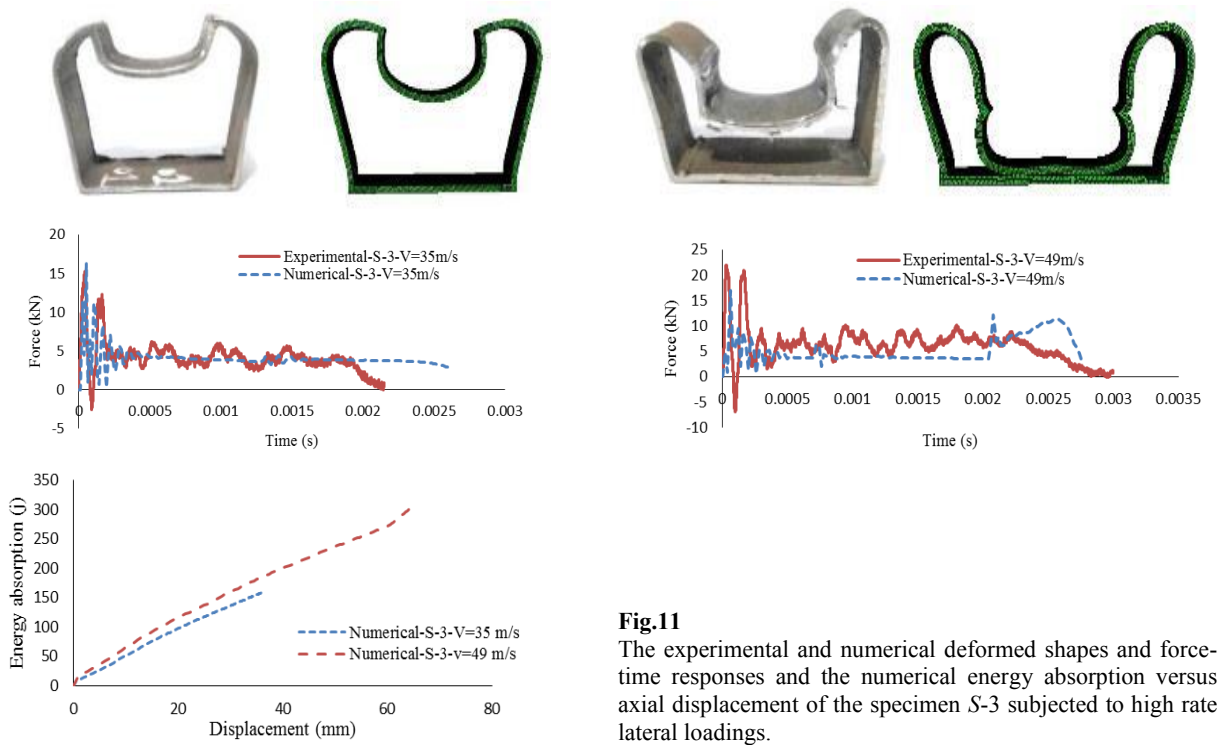

Fig.11
The experimental and numerical deformed shapes and force-time responses and the numerical energy absorption versus axial displacement of the specimen *S*-3 subjected to high rate lateral loadings.

6.1.3 Investigation of loading rate effect

In order to investigate the loading rate effect on the crashworthiness properties of the single square tubes, specimen *S-3* is chosen to be subjected to both dynamic and quasi-static loadings when the other parameters remain unchanged. The experimental force-time curves of the specimen *S-3* for both the quasi-static and dynamic lateral

loading conditions (dynamic loading with the impact velocity of 49 *m/s*) are depicted in Fig. 12. It is revealed that the amount of peak load increases with the increase of loading rate due to the tube material sensitivity to the strain rate which increases by increasing the loading rate from quasi-static condition to dynamic one and therefore the yield stress of the tube material (mild steel) increases as a result. Fig. 12 is also provided to show the experimental deformed shapes of the specimen *S-3* under the quasi-static and dynamic lateral loading conditions.

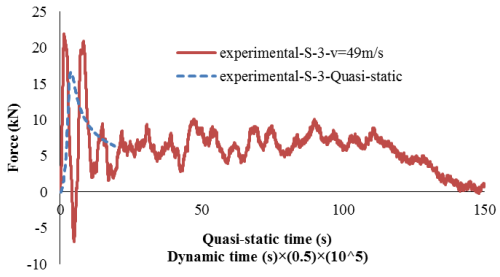

Quasi-static loading condition Dynamic loading condition (*v*=49 *m/s*)

Fig.12
The experimental deformed shapes and force-time curves of the specimen *S*-3 for both the quasi-static and dynamic lateral loading conditions.

6.2 Internally nested square tubes

In this part the deformation mechanism and energy absorption capacity of the nested square tubes which are laterally affected by the quasi-static and dynamic loadings are examined and the experimental and numerical results will be presented in the following.

6.2.1 Quasi-static loading condition

As it is listed in Table 2, all the tubes in the nested systems (the inner and outer tubes) have the same thickness and length of 2 *mm* and 30 *mm*, respectively. It is obvious from Table 2 that there are 3 types of nested tube systems discussed in this section which are the square-square type (*SS*), lozenge-square type (*LS*) and lozenge-lozenge type (*LL*). All the outer tubes' cross sections (whether the square or lozenge form) have the outer side length of 50 *mm* and also all the inner tubes' cross sections (whether the square or lozenge form) have the outer side length of 30 *mm*. In the quasi-static experimental tests, the deformation rate is considered as 20 *mm/min* and the experimental results of the quasi-static tests, are illustrated in Table 3 which contains the experimental amounts of peak load, mean crushing force for 35 *mm* displacement of the upper jaw and axial displacement at peak load. The experimental deformed shapes of the nested tube specimens (*SS*, *LS* and *LL*) under quasi-static lateral loading are presented in Fig. 13. The experimental quasi-static force-displacement and force-time curves for the nested tube specimens *SS*, *LS* and *LL* which are laterally compressed in the universal test machine, are depicted in Fig 14. It can be concluded from the obtained results that the peak load amount occurs in different displacement values depending on the tubes' configurations in the nested systems. For example, in the deformation process of the specimen *SS*, the peak load amount occurs when the outer tube begins to crush the inner one which leads the peak load to happen at a displacement of 16.46 *mm*. Or in the other case example, the peak load amount of the specimen *LS* occurs at the displacement of 36 *mm* when the deformed outer tube begins to press the inner one. It is also revealed that the energy absorption capability of the sample *SS* is more than that of samples *LS* and *LL* when subjected to an equal quasi-static deformation rate in the universal test machine.

S-3 *SS* *LS* *LL*

Fig.13
The experimental deformed shapes of the specimens *S*-3*, SS, LS* and *LL* under quasi-static lateral loading condition.

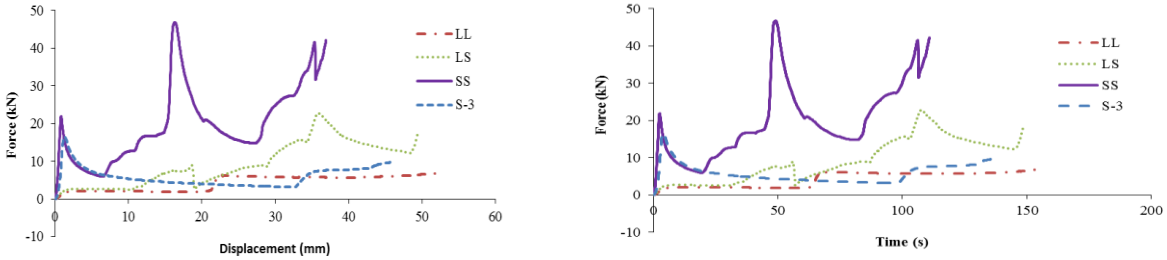

Fig.14
The experimental force-displacement and force-time curves for the specimens *S*-3, *SS*, *LS* and *LL* under quasi-static lateral loading condition.

6.2.2 Dynamic loading condition

This part investigates the dynamic plastic behavior of the nested tube systems (specimens *SS*, *LS* and *LL*) which are laterally impacted, experimentally and numerically. The geometrical properties of the nested specimens are illustrated in Table 2. According to Table 2, the projectile mass is 0.26 *kg* and the impact velocities are 35 *m/s* and 49 *m/s* for each of the nested specimens. Thus, there are six different models which are studied in this part; *SS* under the impact velocities of 35 *m/s* and 49 *m/s*, *LS* under the impact velocities of 35 *m/s* and 49 *m/s*, *LL* under the impact velocities of 35 *m/s* and 49 *m/s*. It should be noted that all the nested specimens have an equal mass of 0.156 *kg*. The experimental and numerical results including the axial displacement, peak load and the mean crushing force are presented in Table 3. The experimental and numerical deformed shapes of the nested tubes after being laterally impacted are shown in Fig. 15. Also, the dynamic experimental and numerical force-time responses for the nested tubes which are laterally impacted in the gas gun, are depicted in Fig. 16, Fig. 17 and Fig. 18 for the specimens *SS*, *LS* and *LL*, respectively. Also, the comparison of experimental dynamic force-time responses of the nested tube specimens for both the velocities of 35 *m/s* and 49 *m/s* are presented in Fig. 19. The numerical energy absorption versus axial displacement for the specimens *SS*, *LS* and *LL* under high rate lateral loadings are also depicted in Fig. 20 for both velocities of 35 *m/s* and 49 *m/s*. It can be revealed that in all the nested tubes, the amount of peak load increases with the increase of impact velocity. Also, all the nested square structures have the appropriate capability to absorb all the input energy in both impact velocities (35 *m/s* and 49 *m/s*) except the model *LL* under the imapct velocity of 49 *m/s*, in which the specimen receives an input energy more than its maximum energy absorption capacity. Furthermore, it is observed that in the nested tube structures, by changing each of the outer or inner tubes or both of them from the square form to lozenge one, the amount of peak load decreases meanwhile the energy absorption capacity decreases too, which is not suitable for energy absorber devices.

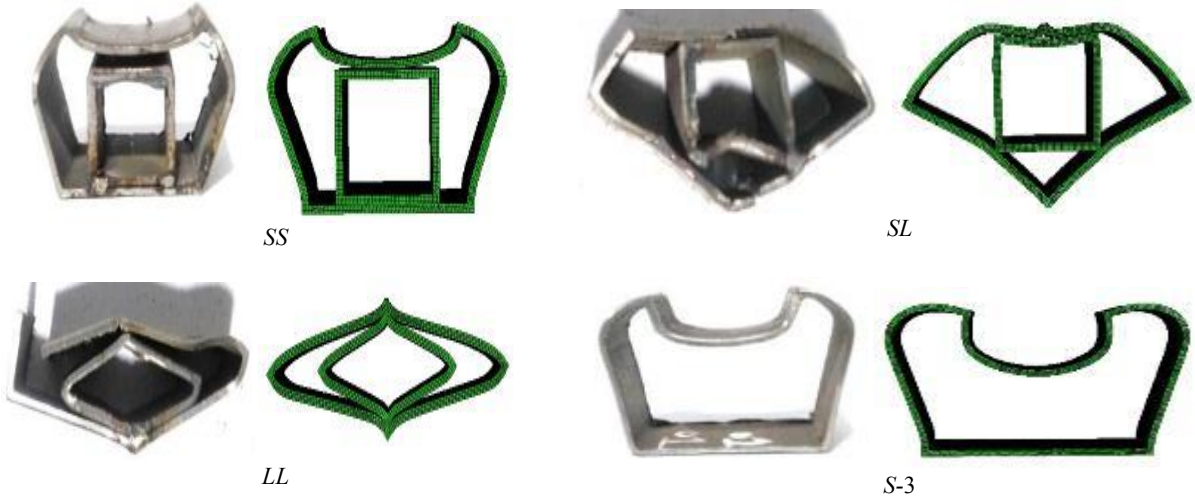

(a) Impact velocity= 35 *m/s*

(b) Impact velocity= 49 *m/s*

Fig.15
The experimental and numerical deformed shapes of the specimens *S*-3, *SS, LS* and *LL* under high rate lateral loadings for impact velocities of (a) 35 *m/s* and (b) 49 *m/s*.

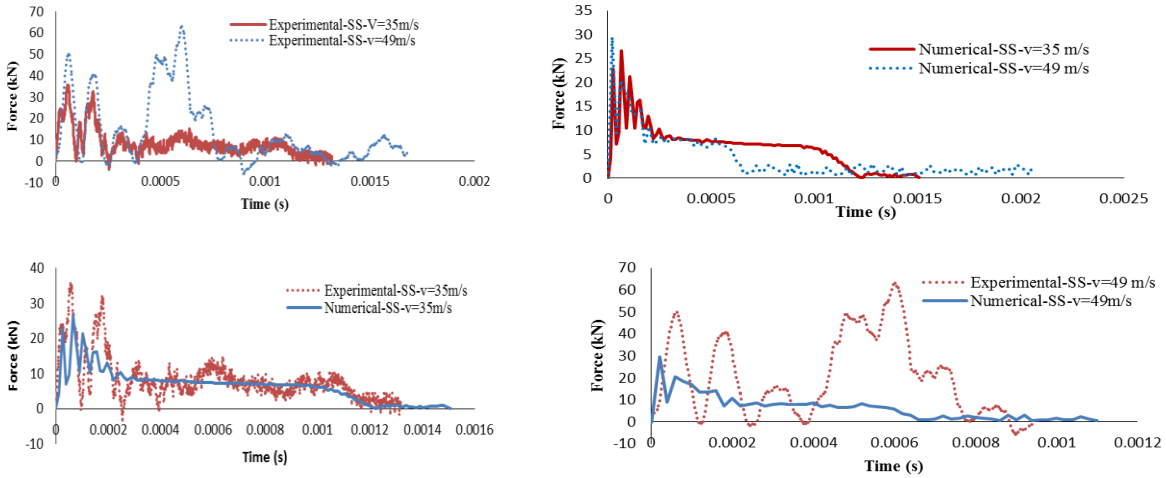

Fig.16
The experimental and numerical force-time responses for the nested tube specimen *SS* under high rate lateral loadings.

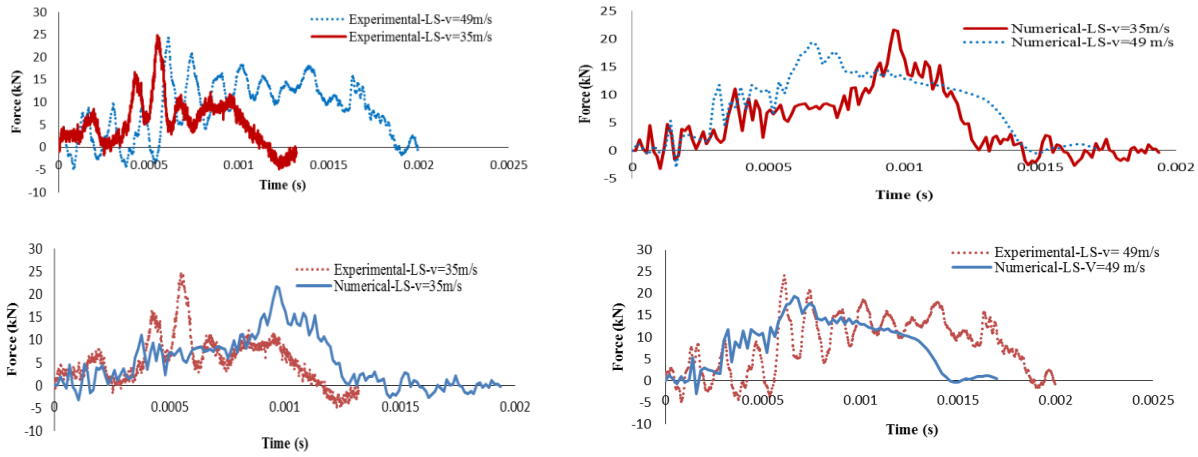

Fig.17
The experimental and numerical force-time responses for the nested tube specimen *LS* under high rate lateral loadings.

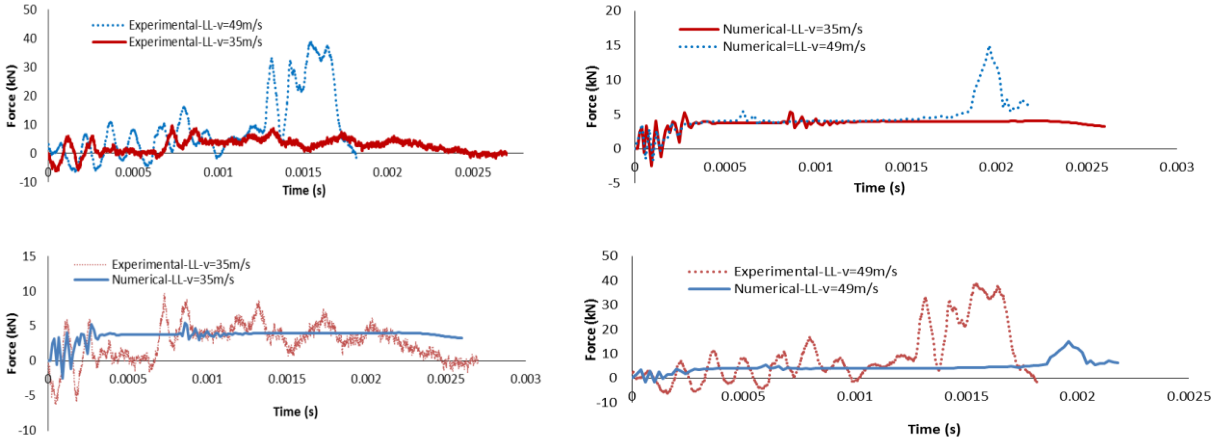

Fig.18
The experimental and numerical force-time responses for the nested tube specimen *LL* under high rate lateral loadings.

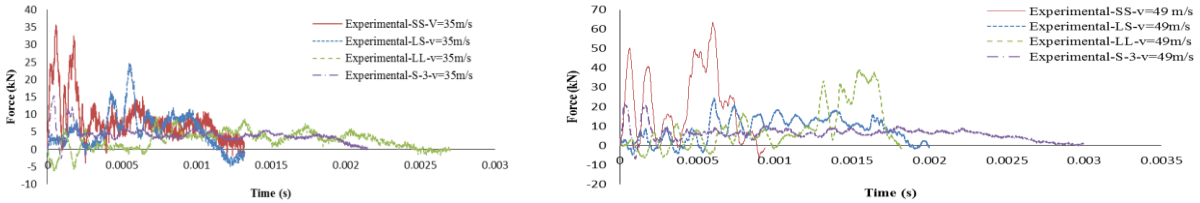

(a) (b)

Fig.19
The comparison of experimental force-time responses for the specimens *S*-3, *SS, LS* and *LL* under high rate lateral loadings for both velocities of (a) 35 *m/s* and (b) 49 *m/s*.

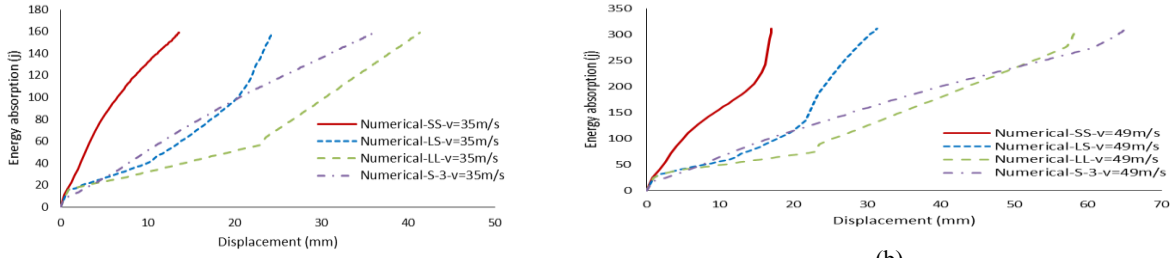

(a) (b)

Fig.20
The comparison of numerical energy absorption versus axial displacement for the specimens *S*-3, *SS, LS* and *LL* under high rate lateral loadings for both velocities of (a) 35 *m/s* and (b) 49 *m/s*.

Table 2
The geometrical properties of the nested square tubes and the quasi-static and dynamic loading conditions.

Model	The properties of the nested square tubes (nested structure mass: 0.156 *kg*)			Quasi-static test	Dynamic test	
	Material	The outer tube	The inner tube			
		wall thickness= 2 *mm*, tube length= 30 *mm*	wall thickness= 2 *mm*, tube length= 30 *mm*			
		Outer side length of the hollow square cross section (*mm*)	Outer side length of the hollow square cross section (*mm*)	Deformation rate (*mm/min*)	Projectile mass (*kg*)	Projectile velocity (*m/s*)
SS	Mild steel	50	30	20	0.26	35 & 49
LS		50	30		0.26	35 & 49
LL		50	30		0.26	35 & 49

6.2.3 Investigation of loading rate effect

In order to investigate the effect of loading rate on the crashworthiness characteristics of the nested square tubes, all three configurations of the nested tubes (*SS*, *LS* and *LL*) are subjected to both lateral quasi-static and dynamic loadings. It is needed to mention that the impact velocity of the dynamic tests which are compared with the quasi-static ones in this section, is chosen to be 49 *m/s*. Fig. 21 presents the experimental force-time curves of the nested tube specimens *SS*, *LS* and *LL* for both the quasi-static and dynamic lateral loading conditions. As it was concluded for the single square tube (sample *S-3*), It can be revealed for the nested square tubes that the amount of peak load increases with the increase of loading rate due to the tube material sensitivity to the strain rate which increases by increasing the loading rate from quasi-static condition to dynamic one and therefore the yield stress of the tube material (mild steel) increases as a result. Fig. 22 compares the experimental deformed shapes of the nested tube specimens in the quasi-static and dynamic lateral loading conditions.

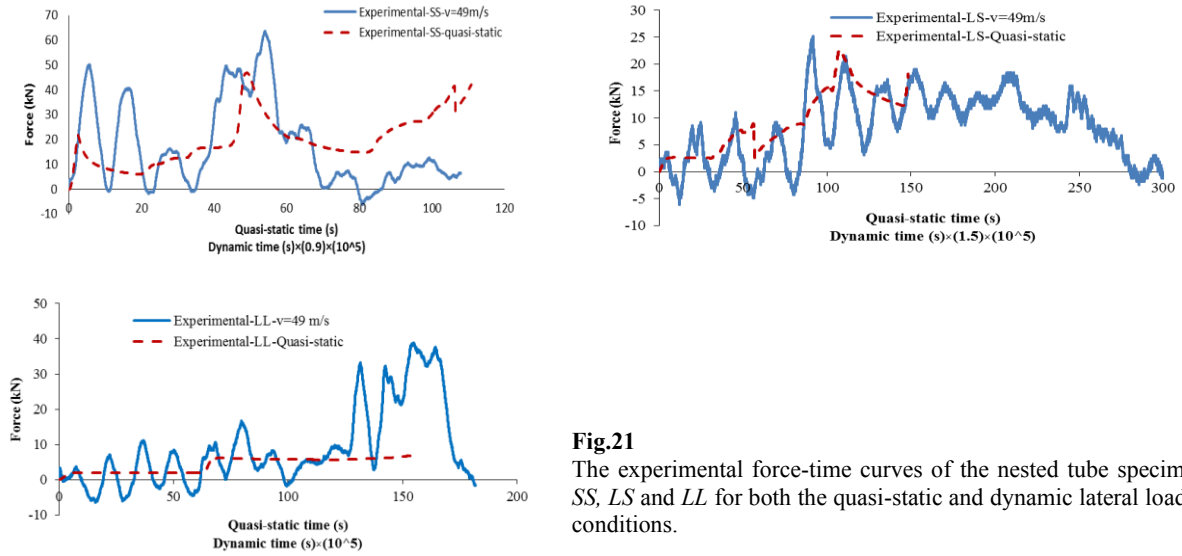

Fig.21
The experimental force-time curves of the nested tube specimens *SS, LS* and *LL* for both the quasi-static and dynamic lateral loading conditions.

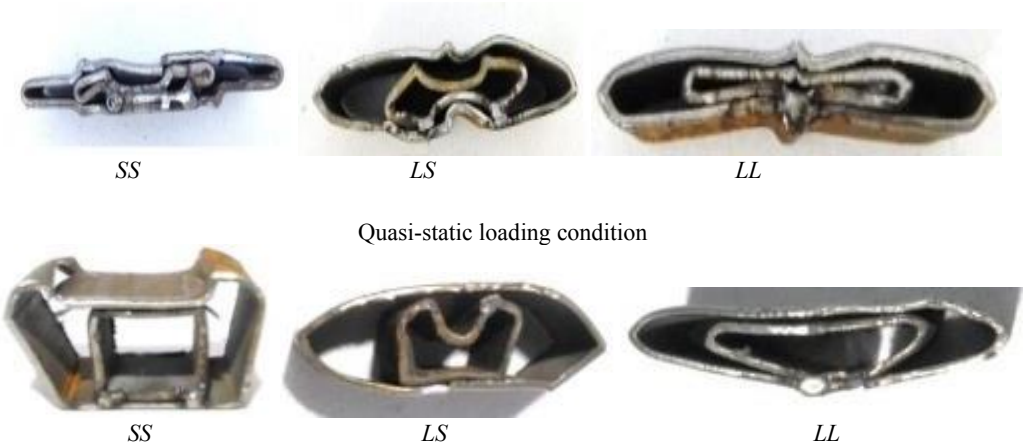

Fig.22
The experimental deformed shapes of the nested tube specimens in the quasi-static and dynamic lateral loading conditions.

6.3 Comparison of single and nested square tubes

Based on the obtained results from the previous sections, one can compare the deformation behavior of the single and nested square tubes both in the quasi-static and high rate loading conditions.

6.3.1 Quasi-static loading condition

In this part the quasi-static experimental results of the specimens *S-3*, *SS*, *LS* and *LL* are compared with each other. As it was mentioned before, all the specimens *S-3*, *SS*, *LS* and *LL* have an equal mass of 0.156 *kg* in order to have a reasonable comparison. All the comparisons in this section are done at the deformation rate of 20 *mm/min* in the universal test machine. It is also needed to mention that the specimen *S-3* in this part, is compressed more than that of mentioned in the previous sections in order to have a better comparison with the the specimens *SS*, *LS* and *LL*. Table 3 is also provided to compare the experimental amounts of peak load, mean crushing force for 35 *mm* displacement of the upper jaw and axial displacement at peak load between the mentioned specimens under the quasi-static lateral loading condition. Fig. 13 gives a comparison between the experimental deformed shapes of the specimens *S-3*, *SS*, *LS* and *LL* under the quasi-static lateral loading condition and Fig. 14 compares the quasi-static behavior of the specimens *S-3*, *SS*, *LS* and *LL* under lateral compression through the force-time and force-displacement curves. It is revealed that the specimens *LS* and *LL* transmit low amounts of forces at the initial stages of deformation process comparing to specimen *S*-3, but in the following when the outer tube of the nested models *LS* and *LL* crushes the inner tube, the amount of force increases and even becomes more than that of the specimen *S-3*. Considering the obtained results, it appears that the nested tube systems act as better energy absorbers comparing to the single tubes, however it is important to notice the tube configurations in the nested systems in order to use the most efficiency of the nested tubes as energy absorbers.

Table 3
The values of axial displacement, peak load and mean crushing force of the single and nested square tubes both under the quasi-static and dynamic loading conditions.

Model	Quasi-static experimental and theoretical results					Dynamic experimental, numerical and theoretical results					
						Impact velocity= 35 (*m/s*)			Impact velocity= 49 (*m/s*)		
	Axial displacement at peak load (*mm*)	Peak load (*kN*)	Mean crushing force (*kN*) for Exp/theori			Axial displacement (*mm*) Exp/Num[b]	Peak load (*kN*) Exp/Num	Mean crushing force (*kN*) Exp/Num/ theori	Axial displacement (*mm*) Exp/Num/	Peak load (*kN*) Exp/Num	Mean crushing force (*kN*) Exp/Num/ theori
			UJD[a]=6.6 (*mm*)	UJD=19 (*mm*)	UJD=35 (*mm*)						
Single square tubes											
S-1	1.02	40.45	19.18/19	---	---	---	---	---	---	---	---
S-2	0.99	22.27	8.59/8.3	---	---	---	---	---	---	---	---
S-3	1.27	16.55	8.81/8.5	---	5.16/5	27/36.17	15.28/16.3	5.9/4.4/4.3	52/65.26	21.9/16.9	6/4.8/4.7
L-1	4.35	2.12	---	1.94/1.7	---	---	---	---	---	---	---
L-2	7.39	1.93	---	1.72/1.5	---	---	---	---	---	---	---
Nested square tubes											
SS	16.33	46.78	---	---	18.82/18.67	11.5/13.6	35.63/26.6	13.8/11.7/10.8	16.5/17.01	63.6/29.4	18.9/18.3/17.6
LS	35.82	22.73	---	---	6.53/6.2	28/24.4	24.87/21.7	5.69/6.53/4.7	38/31.36	24.3/19.4	8.21/9.95/7.86
LL	51.91	6.85	---	---	3.44/3.1	36.5/41.35	9.67/5.37	4.36/3.85/3.1	46.5/58.31	38.9/15	6.7/5.4/5.2

[a] UJD: Upper Jaw Displacement (in the universal test machine)
[b] Exp/Num: Experimental/Numerical

6.3.2 Dynamic loading condition

This part represents a comparison between the obtained dynamic experimental results of the specimens *S-3*, *SS*, *LS* and *LL* for the impact velocities of 35 *m/s* and 49 *m/s*. It is also needed to remember that all the specimens *S-3*, *SS*, *LS* and *LL* have an equal mass of 0.156 *kg* in order to have a reasonable comparison. Table 3 compares the amounts of peak load, mean crushing force and axial displacement of the mentioned specimens with each other. Fig. 15 shows the experimental and numerical deformed shapes of the specimens *S-3*, *SS*, *LS* and *LL* after being laterally impacted in the gas gun and Fig. 19 and Fig. 20 are also provided to compare the dynamic behavior of the laterally impacted specimens *S-3*, *SS*, *LS* and *LL* with each other via the force-time and energy absorption curves for both the impact velocities of 35 *m/s* and 49 *m/s*. It is concluded that despite the single square tube specimen (*S-3*) which has a uniform behavior after the initial peak load, the nested square tubes (specimens *SS*, *SL* and *LL*) have a different behavior which means that the outer tube of the nested system absorbs energy until it begins to crush the inner tube and that's the time in which the amount of force increases due to the effect of the inner tube on energy absorption process. In the comparison of *SS* and *S-3* specimens, it is observed that the amount of initial peak load and the energy absorption capability of the specimen SS are more than those of the *S-3* specimen. It is also observed that in the comparison of *LL* and *S-3* specimens, the amount of initial peak load and the energy absorption capability of the specimen *LL* are less than those of the *S-3* specimen. Also, comparing the specimens *LS* and *S-3* results in the fact

that the amount of initial peak load in the *LS* specimen is less than that of the *S-3* specimen but the energy absorption capability is almost equal for both of them.

7 CONCLUSION

This paper investigated the dynamic and quasi-static plastic behavior of the single and internally nested square tubes which were subjected to lateral loadings, experimentally and numerically. The high rate and the quasi-static experimental tests were conducted in a gas gun and in a universal test machine, respectively. Also, the numerical results were obtained using the finite element software Abaqus. Comparison of dynamic results from both experiment and finite element simulation methods has been made. The numerical results were found to quite satisfactory in comparison to those of experiments. It was concluded that in the single square tubes, the amount of peak load decreases by increasing the side length amount of the tube hollow square cross section. It was also revealed that the amount of peak load decreases significantly when the form of the single tube changes from square to lozenge. Although the reduction of peak load amount is desirable in energy absorber devices, but the energy absorption capability is another important parameters in the energy absorbers which should be considered accurately. From the obtained results, it was found that by changing the form of the single tube from square to lozenge, the single tube as an energy absorber loses its capability of energy absorption significantly. It was also observed that in the nested tube structures, by changing each of the outer or inner tubes or both of them from the square form to lozenge one, the amount of peak load decreases meanwhile the energy absorption capacity decreases too especially when both of the outer and inner tubes of the nested system are in the lozenge form.

ACKNOWLEDGEMENTS

The authors would like to acknowledge Prof. Ablofazl Darvizeh who passed away on March 6, 2021. We deeply appreciate not only his constant scientific supports in this research but also his kindness, patience, morality, and comprehensiveness as an inspiring teacher.

REFERENCES

[1] Guler M.A., Cerit M.E., Bayram B., Gerceker B., Karakaya E., 2010, The effect of geometrical parameters on the energy absorption characteristics of thin-walled structures under axial impact loading, *International Journal of Crashworthiness* **15**(4): 377-390.

[2] Pirmohammad S., Marzdashti S.E., 2016, Crushing behavior of new designed multi-cell members subjected to axial and oblique quasi-static loads, *Thin-Walled Structures* **108**: 291-304.

[3] Gao Q., Wang L., Wang Y., Wang C., 2016, Crushing analysis and multiobjective crashworthiness optimization of foam-filled ellipse tubes under oblique impact loading, *Thin-Walled Structures* **100**: 105-112.

[4] Nia A.A., Nejad K.F., Badnava H., Farhoudi H.R., 2012, Effects of buckling initiators on mechanical behavior of thin-walled square tubes subjected to oblique loading, *Thin-Walled Structures* **59**: 87-96.

[5] Abramowicz W., Jones N., 1986, Dynamic progressive buckling of circular and square tubes, *International Journal of Impact Engineering* **4**(4): 243-270.

[6] Simhachalam B., Srinivas K., Rao C.L., 2014, Energy absorption characteristics of aluminium alloy AA7XXX and AA6061 tubes subjected to static and dynamic axial load, *International Journal of Crashworthiness* **19**(2): 139-152.

[7] Yalçın M.M., Genel K., 2019, On the axial crush performance of PVC foam-filled aluminum/CFRP hybrid circular tube, *Sakarya Üniversitesi Fen Bilimleri Enstitüsü Dergisi* **23**(6): 1154-1162.

[8] Kahraman Y., Akdikmen O., 2021, Experimental investigation on deformation behavior and energy absorption capability of nested steel tubes under lateral loading, Engineering Science and Technology, *An International Journal* **24**(2): 579-588.

[9] Shabani B., Rad S.G., Alijani A., Darvizeh A., Rajabiehfard R., 2021, Dynamic plastic behavior of single and nested rings under lateral impact, *Thin-Walled Structures* **160**: 107373.

[10] Morris E., Olabi A.G., Hashmi M.S.J., 2006, Analysis of nested tube type energy absorbers with different indenters and exterior constraints, *Thin-walled structures* **44**(8): 872-885.

[11] Gao Q., Wang L., Wang Y., Wang C., 2017, Multi-objective optimization of a tapered elliptical tube under oblique impact loading, *Proceedings of the Institution of Mechanical Engineers, Part D Journal of Automobile Engineering* **231**(14): 1978-1988.

[12] Olabi A.G., Morris E., Hashmi M.S.J., Gilchrist M.D., 2008, Optimised design of nested oblong tube energy absorbers under lateral impact loading, *International Journal of Impact Engineering* **35**(1): 10-26.

[13] Wu L., Carney III J.F., 1998, Experimental analyses of collapse behaviors of braced elliptical tubes under lateral compression, *International Journal of Mechanical Sciences* **40**(8): 761-777.

[14] Tran T.N., Ton T.N.T., 2016, Lateral crushing behaviour and theoretical prediction of thin-walled rectangular and square tubes, *Composite Structures* **154**: 374-384.

[15] Zhang B., Wang L., Zhang J., Jiang Y., Wang W., Wu G., 2021, Deformation and energy absorption properties of cenosphere/aluminum syntactic foam-filled circular tubes under lateral quasi-static compression, *International Journal of Mechanical Sciences* **192**: 106126.

[16] Wang H., Yang J., Liu H., Sun Y., Yu T.X., 2015, Internally nested circular tube system subjected to lateral impact loading, *Thin-Walled Structures* **91**: 72-81.

[17] Tran T., 2018, A study on nested two-tube structures subjected to lateral crushing, *Thin-Walled Structures* **129**: 418-428.

[18] Yang X., Ma J., Sun Y., Yang J., 2019, An internally nested circular-elliptical tube system for energy absorption, *Thin-Walled Structures* **139**: 281-293.

[19] Baroutaji A., Gilchrist M.D., Olabi A.G., 2016, Quasi-static, impact and energy absorption of internally nested tubes subjected to lateral loading, *Thin-Walled Structures* **98**: 337-350.

[20] Xu B., Wang C., Xu W., 2019, An efficient energy absorber based on fourfold-tube nested circular tube system, *Thin-Walled Structures* **137**: 143-150.

[21] Yu Z.L., Xue P., Chen Z., 2017, Nested tube system applicable to protective structures against blast shock, *International Journal of Impact Engineering* **102**: 129-139.

[22] Hu J., Lu G., Yang H., Yu T.X., Xu J., 2017, Dynamic response of internally nested hemispherical shell system to impact loading, *Thin-Walled Structures* **120**: 29-37.

[23] Remennikov A.M., Kong S.Y., Uy B., 2011, Response of foam-and concrete-filled square steel tubes under low-velocity impact loading, *Journal of Performance of Constructed Facilities* **25**(5): 373-381.

[24] Linul E., Movahedi N., Marsavina L., 2018, On the lateral compressive behavior of empty and ex-situ aluminum foam-filled tubes at high temperature, *Materials* **11**(4): 554.

[25] Hanssen A.G., Hopperstad O.S., Langseth M., 2001, Design of aluminium foam-filled crash boxes of square and circular cross-sections, *International Journal of Crashworthiness* **6**(2): 177-188.

[26] Hou S., Li Q., Long S., Yang X., Li W., 2009, Crashworthiness design for foam filled thin-wall structures, *Materials & Design* **30**(6): 2024-2032.

[27] Gupta N.K., Sekhon G.S., Gupta P.K., 2001, A study of lateral collapse of square and rectangular metallic tubes, *Thin-Walled Structures* **39**(9): 745-772.

[28] Gupta N.K., Sekhon G.S., Gupta P.K., 2005, Study of lateral compression of round metallic tubes, *Thin-Walled Structures* **43**(6): 895-922.

[29] Baroutaji A., Gilchrist M.D., Smyth D., Olabi A.G., 2015, Crush analysis and multi-objective optimization design for circular tube under quasi-static lateral loading, *Thin-Walled Structures* **86**: 121-131.

[30] Sadeghi H., Davey K., Darvizeh R., Rajabiehfard R., Darvizeh A., 2020, An investigation into finite similitude for high-rate loading processes: Advantages in comparison to dimensional analysis and its practical implementation, *International Journal of Impact Engineering* **140**: 103-554.

[31] Sadeghi H., Davey K., Darvizeh R., Darvizeh A., 2019, A scaled framework for strain rate sensitive structures subjected to high rate impact loading, *International Journal of Impact Engineering* **125**: 229-245.

[32] Sadeghi H., Davey K., Darvizeh R., Darvizeh A., 2019, Scaled models for failure under impact loading, *International Journal of Impact Engineering* **129**: 36-56.

[33] Davey K., Sadeghi H., Darvizeh R., Golbaf A., Darvizeh A., 2021, A finite similitude approach to scaled impact mechanics, *International Journal of Impact Engineering* **148**: 103744.

[34] Senthil K., Iqbal M.A., Bhargava P., Gupta N.K., 2017, Experimental and numerical studies on mild steel plates against 7.62 API projectiles, *Procedia Engineering* **173**: 369-374.

[35] Rajabiehfard R., Darvizeh A., Darvizeh M., Ansari R., Alitavoli M., Sadeghi H., 2016, Theoretical and experimental analysis of elastic–plastic cylindrical shells under two types of axial impacts, *Thin-Walled Structures* **107**: 315-326.

[36] Rajabiehfard R., Darvizeh A., Darvizeh M., Ansari R., Sadeghi H., 2015, Effects of boundary and loading conditions on the dynamic plastic buckling of cylindrical shells under axial impact, *Modares Mechanical Engineering* **15**(2): 281-288.

[37] Rajabieh Fard R., Darvizeh A., Darvizeh M., Ansari R., Sadeghi H., 2016, Effect of strain hardening modulus on buckling of elastic-plastic cylindrical shells, due to the axial impact, *Iranian Journal of Mechanical Engineering* **18**(1): 91-114.

[38] Alitavoli M., Sadeghi H., Mosavi S.M., Rajabiehfard R., 2018, Experimental and numerical analysis of dynamic plastic behavior of long metallic bars under axial impact, *Computations and Simulations in Mechanical Science* **1**(1): 1-11.

[39] Chen W. , Wierzbicki T., 2001, Relative merits of single-cell, multi-cell and foam-filled thin-walled structures in energy absorption, *Thin-Walled Structures* **39**: 287-306 .

[40] Tran T., Hou S., Han X., Nguyen N., Chau M., 2014, Theoretical prediction and crashwor- thiness optimization of multi-cell square tubes under oblique impact loading, *International Journal of Mechanical Sciences* **89**: 177-193 .

[41] Abramowicz W., Jones N., 1984, Dynamic axial crushing of square tubes, *International Journal of Impact Engineering* **2**:179-208 .

[42] Fan H., Luo Y., Yang F., Li W., 2018, Approaching perfect energy absorption through struc- tural hierarchy, *International Journal of Engineering Science* **130**: 12-32 .